

Silicon-based optoelectronic synaptic devices

Lei Yin(尹蕾), Xiaodong Pi(皮孝东), Deren Yang(杨德仁)

Citation: Chin. Phys. B . 2020, 29(7): 070703 . **doi:** 10.1088/1674-1056/ab973f
Journal homepage: http://cpb.iphy.ac.cn; http://iopscience.iop.org/cpb

What follows is a list of articles you may be interested in

High-performance synaptic transistors for neuromorphic computing

Hai Zhong(钟海), Qin-Chao Sun(孙勤超), Guo Li(李果), Jian-Yu Du(杜剑宇), He-Yi Huang(黄河意), Er-Jia Guo(郭尔佳), Meng He(何萌), Can Wang(王灿), Guo-Zhen Yang(杨国桢), Chen Ge(葛琛), Kui-Juan Jin(金奎娟)

Chin. Phys. B . 2020, 29(4): 040703 . **doi:** 10.1088/1674-1056/ab7806

Preliminary abnormal electrocardiogram segment screening method for Holter data based on long short-term memory networks

Siying Chen(陈偲颖), Hongxing Liu(刘红星)

Chin. Phys. B . 2020, 29(4): 040701 . **doi:** 10.1088/1674-1056/ab6d52

Multiple Lagrange stability and Lyapunov asymptotical stability of delayed fractional-order Cohen-Grossberg neural networks

Yu-Jiao Huang(黄玉娇), Xiao-Yan Yuan(袁孝焰), Xu-Hua Yang(杨旭华), Hai-Xia Long(龙海霞), Jie Xiao(肖杰)

Chin. Phys. B . 2020, 29(2): 020703 . **doi:** 10.1088/1674-1056/ab6716

Coexistence and local Mittag-Leffler stability of fractional-order recurrent neural networks with discontinuous activation functions

Yu-Jiao Huang(黄玉娇), Shi-Jun Chen(陈时俊), Xu-Hua Yang(杨旭华), Jie Xiao(肖杰)

Chin. Phys. B . 2019, 28(4): 040701 . **doi:** 10.1088/1674-1056/28/4/040701

Synthesization of high-capacity auto-associative memories using complex-valued neural networks

Yu-Jiao Huang(黄玉娇), Xiao-Yan Wang(汪晓妍), Hai-Xia Long(龙海霞), Xu-Hua Yang(杨旭华)

Chin. Phys. B . 2016, 25(12): 120701 . **doi:** 10.1088/1674-1056/25/12/120701

TOPICAL REVIEW — Physics in neuromorphic devices

Silicon-based optoelectronic synaptic devices*

Lei Yin(尹蕾), Xiaodong Pi(皮孝东)†, and Deren Yang(杨德仁)‡

State Key Laboratory of Silicon Materials and School of Materials Science and Engineering, Zhejiang University, Hangzhou 310027, *China*

(Received 2 April 2020; revised manuscript received 25 May 2020; accepted manuscript online 28 May 2020)

High-performance neuromorphic computing (i.e., brain-like computing) is envisioned to seriously demand optoelectronically integrated artificial neural networks (ANNs) in the future. Optoelectronic synaptic devices are critical building blocks for optoelectronically integrated ANNs. For the large-scale deployment of high-performance neuromorphic computing in the future, it would be advantageous to fabricate optoelectronic synaptic devices by using advanced silicon (Si) technologies. This calls for the development of Si-based optoelectronic synaptic devices. In this work we review the use of Si materials to make optoelectronic synaptic devices, which have either two-terminal or three-terminal structures. A series of important synaptic functionalities have been well mimicked by using these Si-based optoelectronic synaptic devices. We also present the outlook of using Si materials for optoelectronic synaptic devices.

Keywords: silicon, optoelectronic synaptic devices, neuromorphic computing

PACS: 07.05.Mh, 42.79.Ta, 72.20.Jv **DOI:** 10.1088/1674-1056/ab973f

1. Introduction

A brain is the most powerful information processor in nature.[1] An interconnected neural network in a brain is capable of distributed parallel processing, enabling high-speed computing. Moreover, both information processing and memory can take place in a brain, avoiding the data transfer between memory and processors in the current mainstream computing based on the von Neumann structure.[2] Hence, a brain consumes rather low energy.[3–5] Now it is widely believed that neuromorphic computing (i.e., brain-like computing) is one of the most important choices for next-generation computing. Since synapses play a critical role in a neural network, artificial synapses (i.e., synaptic devices) are thought to be crucial building blocks for neuromorphic computing.

Researchers have been investigating synaptic devices for many years. Synaptic devices based on the complementary metal–oxide–semiconductor (CMOS) technology of silicon (Si) were initially developed.[6–9] These devices did not have the capability of inherent hardware-based memorizing. The imitation of synaptic functionalities was mainly achieved by designing complex analog circuits.[10–12] Memristors were then used as synaptic devices, which possessed both processing and memorizing functions.[13–16] Although they demonstrated great potential for emulating synaptic functionalities,[17–19] memristors needed to face the trade-off among bandwidth, connection, and density.[20] It has been realized that the incorporation of light into synaptic devices can offer advantages such as ultrafast computing, high bandwidth, robustness, and low power consumption.[21–26] Light may enable real-time sensing, which helps to realize the functionalities of a visual nervous system by using synaptic devices.[27–31] Hence, optoelectronic synaptic devices working with light have recently attracted great attention. Various materials such as metal oxide films,[32–38] carbon nanotubes,[39–42] perovskite,[43–48] and two-dimensional layered materials[49–54] have been employed to fabricate optoelectronic synaptic devices with two- or three-terminal structures.

Si has evolved to be the material of choice for very large-scale integration (VLSI) circuits, on which the amazing success of current mainstream computing is based. If Si is used to make optoelectronic synaptic devices, the advanced mature technology of Si together with the low cost of Si should significantly contribute to the development of optoelectronically integrated neural network, which may be seriously demanded by the large-scale deployment of neuromorphic computing based on optoelectronic integration in the future. In this work we review the progress of using Si for optoelectronic synaptic devices. Before the discussion on the two- and three-terminal Si-based optoelectronic devices, we first briefly introduce biological synapses and synaptic plasticity. The opportunities and challenges for the development of Si-based optoelectronic

*Project supported by the National Key Research and Development Program of China (Grant Nos. 2017YFA0205704 and 2018YFB2200101), the National Natural Science Foundation of China (Grant Nos. 91964107 and 61774133), the Fundamental Research Funds for the Central Universities, China (Grant No. 2018XZZX003-02), the National Natural Science Foundation of China for Innovative Research Groups (Grant No. 61721005), and the Zhejiang University Education Foundation Global Partnership Fund.

†Corresponding author. E-mail: xdpi@zju.edu.cn

‡Corresponding author. E-mail: mseyang@zju.edu.cn

© 2020 Chinese Physical Society and IOP Publishing Ltd

synaptic devices in the future are also presented.

2. Biological synapses

A brain consists of approximately 10^{11} neurons. Each neuron is connected to other neurons via approximately 10^3–10^4 synapses.[3,4] Figure 1 schematically illustrates signal transmission between neurons through a synapse. The signal transmission starts with the triggering of action potentials in the presynaptic neuron. When the potential reaches a threshold of −55 mV, depolarization of the presynaptic membrane would happen, turning on the voltage-gated calcium (Ca^{2+}) channels. The influx of Ca^{2+} can induce the break of vesicles and release neurotransmitters onto the synaptic cleft. With the receptors on the postsynaptic neuron blinded by neurotransmitters, depolarizing or hyperpolarizing of the postsynaptic membrane would happen, resulting in the change of the postsynaptic current or potential.[55–57] The postsynaptic current or potential can be divided into excitatory/inhibitory postsynaptic current (EPSC/IPSC) or potential (EPSP/IPSP), depending on the type of the released neurotransmitters. The sum of EPSCs/IPSCs from all kinds of synapses in the postsynaptic neuron determines whether the postsynaptic neuron could activate the potential or not.[58]

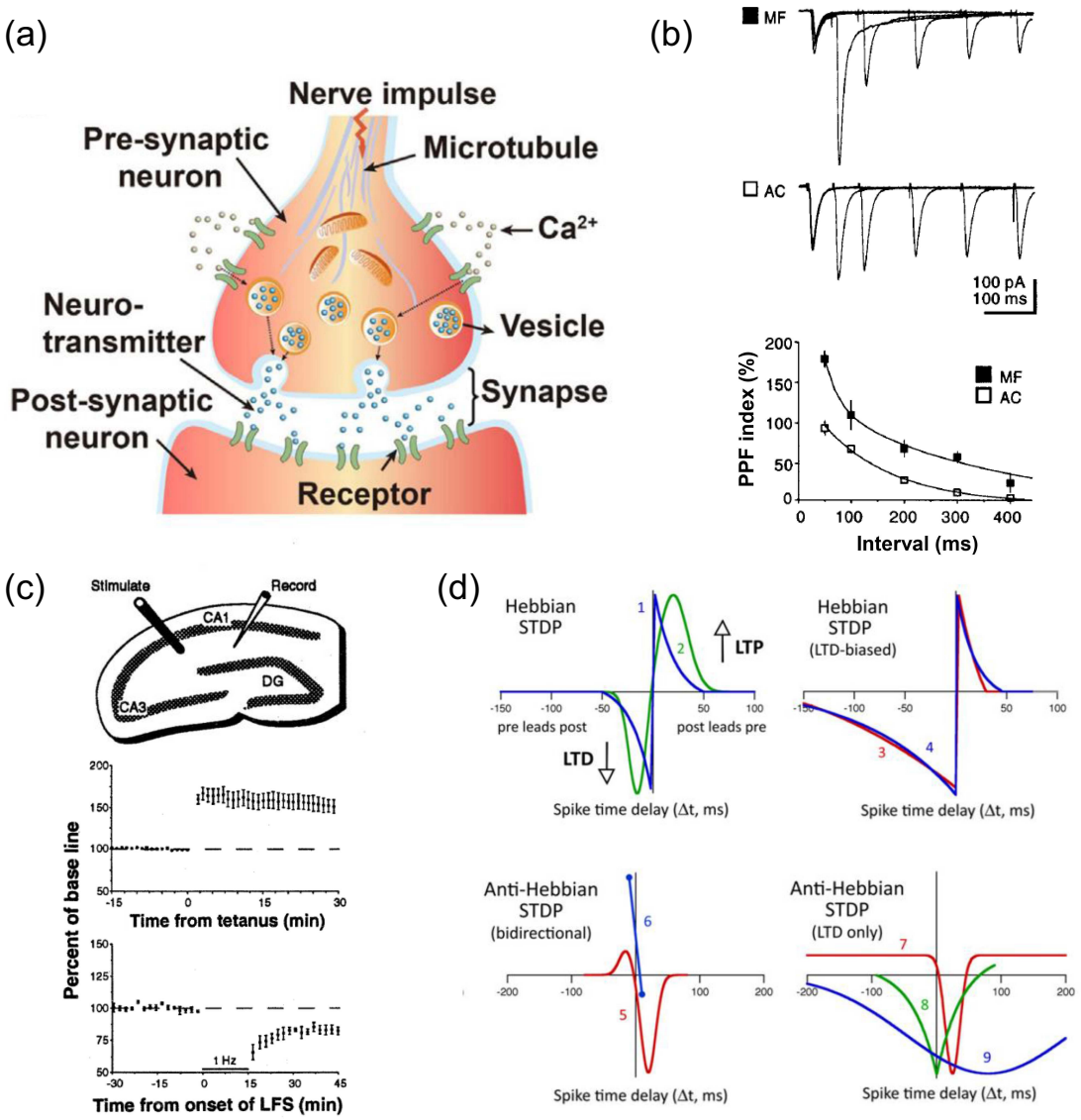


Fig. 1. (a) A Schematic illustration of biological synaptic transmission. Signals are transmitted from the pre-synaptic neuron to the post-synaptic neuron via the neurotransmitter. Reproduced with permission from Ref. [61]. Copyright 2019, Elsevier Ltd. (b) PPF of a mossy fiber (MF) synapse and a assoc/com (AC) synapse. Current traces: superimposed sweeps with five different interstimulus intervals. The graph shows the average PPF index plotted against interstimulus intervals. The points for the AC synapse were fitted with a single exponential ($t = 133$ ms), while the points for the MF synapses were fitted with a double exponential ($t_1 = 27$ ms, $t_2 = 301$ ms). Adapted with permission from Ref. [59]. Copyright 1996, National Academy of Sciences. (c) Experiments illustrating NMDAR-dependent long-term potentiation and long-term depression of hippocampal CA1 synapses. Top: configuration of stimulation and recording. Middle: average change of the response magnitude after high-frequecny (e.g., 100 Hz) stimulations. Bottom: average change of the response magnitude after low-frequency (e.g., 1 Hz) stimulations. Reproduced with permission from Ref. [62]. Copyright 1993, American Association for the Advancement of Science. (d) Typical forms of STDP indicated by nine different curves. Reproduced with permission from Ref. [63]. Copyright 2012, Elsevier Ltd.

The EPSC/IPSC is of significance for information processing, learning, and memory. The magnitude of EPSC/IPSC is determined by the connection strength (i.e., synaptic weight) of a synapse. The synaptic weight is closely related to the activity history of either or both sides of the synapse. The change (potentiation or depression) of the synaptic weight is called synaptic plasticity.[24] There are short-term plasticity (STP) and long-term plasticity (LTP). The STP usually occurs in the time frame of milliseconds to minutes, while the LTP lasts several hours or longer. Paired-pulse facilitation (PPF)/depression (PPD) is a typical STP, which is signified by the potentiation/depression of the postsynaptic current for a second stimulus. Figure 1(b) shows the PPF of a mossy fiber (MF) synapse and an associational/commissural (AC) synapse.[59] Both of the two synapses are excitatory synapses in the hippocampus. The PPF index is defined as

$$\text{PPF index} = [(p_2 - p_1)/p_1] \times 100\%,$$

where p_1 and p_2 are the amplitudes of the EPSC evoked by the first and second stimulus, respectively. It is clear that the PPF index decays with the increase of the time interval (Δt) between two consecutive stimuli. The decay of the PPF index for the MF (AC) synapse may be fitted by using a double (single) exponential. The PPF index of the MF synapse is 2-fold greater than that of the AC synapse when the time interval is small. For the MF synapse, the PPF index shows fast decay when the interval is less than 100 ms, following the double exponential decay relation. Please note the PPF index may be also defined as the ratio of p_2 to p_1.[60]

Spike-rate-dependent synaptic plasticity (SRDP) is a typical type of LTP.[64,65] The firing frequency of the presynaptic spikes readily affects the LTP. For example, low frequency (1–5 Hz) spikes may lead to long-term depression, while high frequency (20–100 Hz) spikes may render long-term potentiation.[66] Figure 1(c) shows the dependence of the long-term potentiation and long-term depression on N-methyl-D-aspartate (NMDA) receptors at the hippocampal CA1 synapses of an adult rat. High-frequency (e.g., 100 Hz) stimulations induce the long-term potentiation, while low-frequency (e.g., 1 Hz) stimulations produce the long-term depression.[62] The LTP also depends on the quantity of stimulations. When the quantity of stimulations increases, the magnitude of the potentiation or depression increases due to the increase of intracellular Ca^{2+} loading.[67,68] Spike-timing-dependent synaptic plasticity (STDP) is critical to the well-known Hebbian theory, which is widely used in the models of circuit-level plasticity, development, and learning.[63] For STDP, the synaptic weight can be modulated by the order and temporal interval of the presynaptic and postsynaptic spikes.[69] Figure 1(d) shows several typical forms of STDP including the Hebbian and anti-Hebbian STDP. For the Hebbian STDP, the long-term potentiation and depression are symmetric in quadrants I and III (plots 1 and 2). Or some of them are biased toward the long-term depression (plots 3 and 4). The long-term potentiation (depression) usually occurs when presynaptic spikes come before (after) postsynaptic spikes. For the Anti-Hebbian STDP, the long-term depression dominates in most cases (plots 7–9), although the long-term potentiation may occur when the postsynaptic spikes precede presynaptic spikes in some cases (plots 5 and 6).

3. Si-based optoelectronic synaptic devices

In optoelectronic synaptic devices, photoelectric conversion is efficiently utilized. Both optical and electrical spikes can be used for optoelectronic synaptic devices. Optical spikes are generally regarded as the stimulations from presynaptic neurons or external environment. Recently, optical signals have also been demonstrated to act as postsynaptic outputs.[70,71] When optoelectronic synaptic devices are fabricated, they have either two-terminal[72,73] or three-terminal structures.[74–76] Various operations may be realized by using these devices, which should help the construction of complex artificial neural networks (ANNs). Here we review Si-based optoelectronic synaptic devices by categorizing them into two-terminal and three-terminal ones.

3.1. Two-terminal synaptic devices

Two-terminal synaptic devices are usually fabricated to build a crossbar array. The simple structure of two-terminal synaptic devices is quite suitable for the high-density integration of ANNs. This has encouraged the recent hardware implementation of ANNs with outstanding on-chip training performance.[77] Two-terminal synaptic devices are often purely electronic.[78] However, light has already been incorporated into two-terminal synaptic devices, enabling the integration of real-time sensing, processing, and memory functions. The resulting two-terminal optoelectronic devices now hold great promise for the development of neuromorphic computing based on optoelectronically integrated artificial neural networks.[73]

In late 1980s, AT&T Bell Laboratories demonstrated optically programmable neural networks based on photoconductive hydrogenated amorphous Si (a-Si:H) arrays.[79–82] The first generation of photoconductive a-Si:H arrays had the vertical (or sandwich-type) structure.[79] As shown in Fig. 2(a), photoconductive a-Si:H was sandwiched between orthogonal bottom electrodes (ITO lines) and top electrodes (Ti/Au lines). The resulting array consisted of 120 rows and 120 columns, forming 14400 synaptic devices. Light incident on a-Si:H led to photocurrent and changed the conductivity of a-Si:H. Figure 2(b) shows the current–voltage characteristics of a single device in the array. The asymmetry characteristics indicated

that the top a-Si:H /metal interface was not good for electron injection. Hence, the array worked in forward bias, giving rise to significant photoresponse. Optical programming was carried out for the array, rendering a Hopfield content addressable memory with the capability of storing five 120-bit memory vectors.

Due to the fact that the vertical arrays could seriously suffer from the point and line defects of a-Si:H, the AT&T Bell Laboratories subsequently developed the second generation of optically programmable synaptic arrays based on a planar (or gap-cell type) structure.[80–82] As schematically shown in Fig. 2(c), the current flowing in the planar structure was parallel to the a-Si:H surface. Optical programming of the planar photoconductor could be carried out by illuminating the exposed a-Si:H area defined by the electrodes. The resulting optically programmable synapses were incorporated into an ANN, as shown in Fig. 2(d). Analog inputs, hidden neurons, and output neurons were also in the network. Adaptive learning based on standard backpropagation techniques was executed by using this network. The dependence of the average errors of the network obtained with either the hardware implementation or software simulation on the quantity of learning trials is shown in Fig. 2(e). The steady-state errors from the hardware implementation were $< 4\%$, similar to those from the software simulation.

Chen *et al.*[83] have recently demonstrated optoelectronic synaptic devices based on the heterostructure of hafnium metal oxide (HfO_2) and bulk Si. The two-terminal device structure is schematically shown in Fig. 3(a). Presynaptic and postsynaptic electrical spikes were designed to enable the demonstration of optically modulated STDP (Figs. 3(b) and 3(c)). Electrical spikes applied at the Si electrode were regarded as presynaptic spikes, which were coupled with optical spikes.

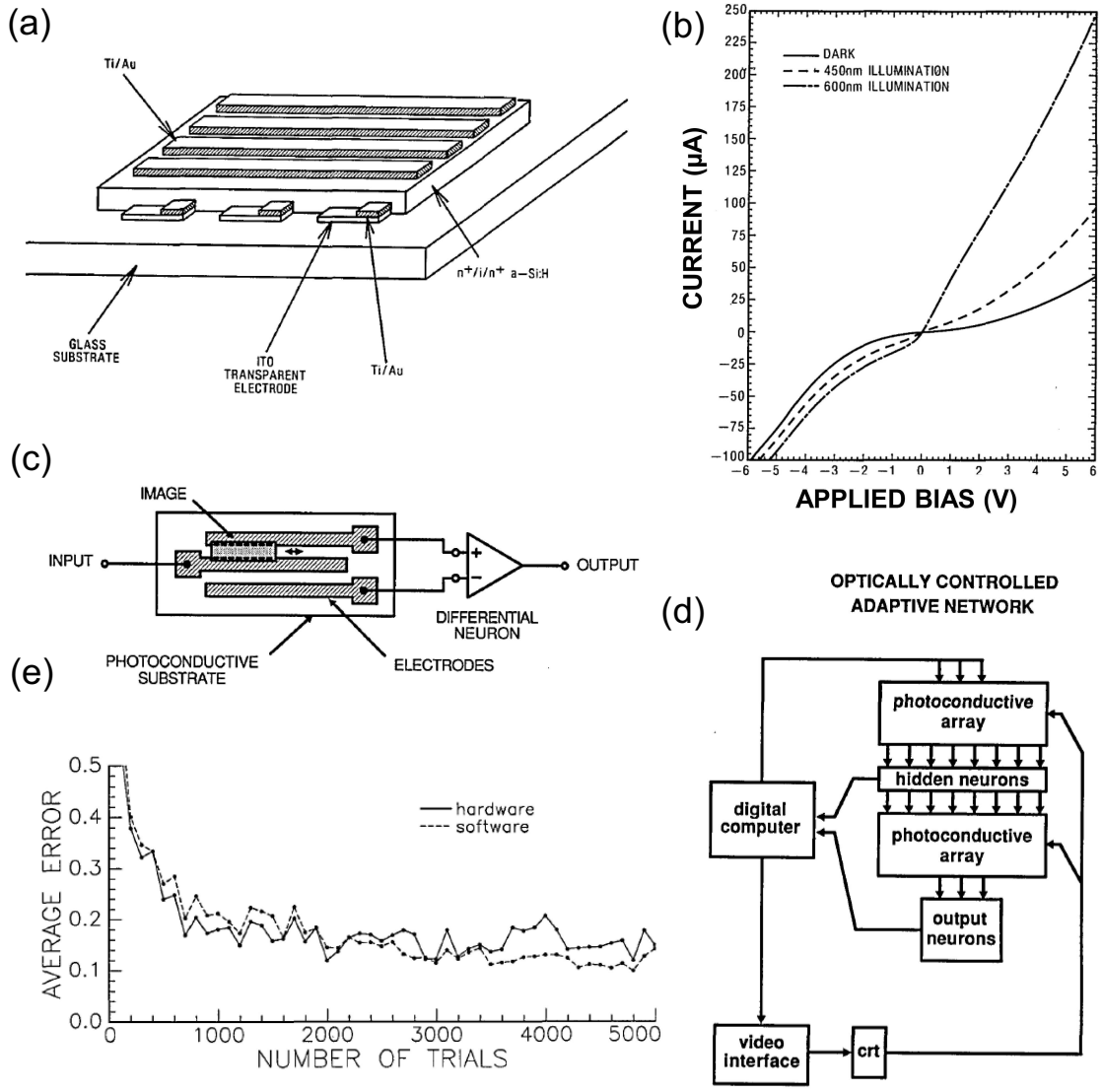


Fig. 2. (a) Schematic of a vertical amorphous Si photoconductive array. (b) Current–voltage characteristics of an individual synapse. The illumination intensity was appropriate 1 mW/cm^2. Bias was applied to the top Ti/Au electrode. Reproduced with permission from Ref. [79]. Copyright 1989, Optical Society of America. (c) Basic configuration of the optically controlled planar photoconductive synapses. (d) Block diagram of the overall hardware network. (e) Average errors number of learning trials for both the hardware network and its software equivalent for the example signal prediction problem. Reproduced with permission from Ref. [82]. Copyright 1991, Optical Society of America.

Electrical spikes applied at the Pt electrode were regarded as postsynaptic spikes. The devices exhibited typical Hebbian STDP. In the long-term potentiation region, the change of synaptic weight (ΔSW%) was readily modulated by the power density of light incident on the devices. Figure 3(d) shows the capacitance–voltage (C–V) curves of a typical device under different illumination conditions. Upon illumination, the capacitance of the depletion in the device increased mainly owing to the reduced depletion region. The voltage drop on the oxide layer was also redistributed when the depletion region was further transformed to an inversion region. Hence, the optically adaptive potentiation was observed. Since the surface region of bulk Si could be impacted by illumination, transient optical spikes were also successfully employed to modulate the postsynaptic current. Figure 3(e) shows that the postsynaptic current increased with the increase of the power density of a transient optical spike.

While the Pt/HfO_2/p-Si device showed stateful photoresponses and nonvolatile memory behavior via transient optoelectronic stimulus, the emulation of STP or LTP behaviors was not realized. However, the STDP of the device made it applicable to the existing ANNs based on memristors.[84] The incorporation of optical signals may generalize a broader artificial synaptic system combining sensing and neural processing, which is expected to bear advanced functionalities in light-controlled cognitive and optical neuromorphic hardware.

Ultra-thin memristors with low reverse current are normally required to build high-density 3D stacking neuromorphic chips. He *et al.*[85] chose the 2D layered material of MoS_2 to from a heterostructure with bulk Si. Optoelectronic synaptic devices based on this MoS_2/Si structure were fabricated. The schematic of such a typical device is shown in Fig. 4(a). Less than 1 nm thick native Si oxide was formed between the n-type MoS_2 and p-type bulk Si, acting as an interfacial trapping layer. In the dark, the vertical device exhibited a photodiode-like behavior with a large self-rectification ratio of $\sim 4 \times 10^3$. A persistent photocurrent (PPC) phenomenon could be observed after UV optical stimulations. Upon electrical stimulations the device showed a volatile resistive switching behavior. Therefore, the device could be used to emulate synaptic functionalities. For example, the long-term potentiation (long-term depression) of synapses was emulated with optical (electrical)

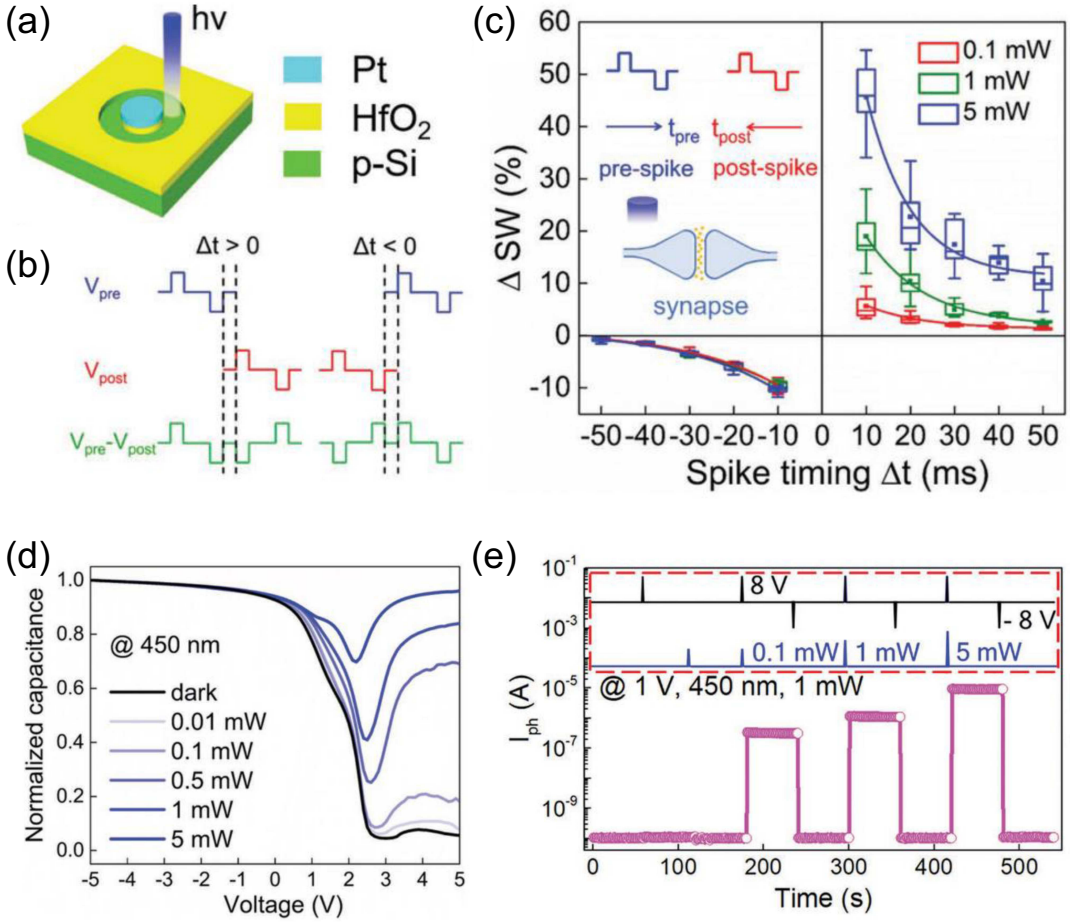


Fig. 3. (a) Schematic of an optoelectronic synaptic device based on the heterostructure of bulk Si and HfO_2. (b) Schematic of electrical spikes for the demonstration of STDP. (c) STDP under different illumination conditions. The postsynaptic current was measured when the presynaptic electrical spike was 5 min before (I_1) or after (I_2) the postsynaptic electrical spike. The relative change of synaptic weight (ΔSW%) was defined as $(I_2 - I_1)/I_1$. (d) C–V characteristics under different illumination conditions. (e) Multilevel photocurrent (I_{ph}) output after the device was regulated by electrical spikes under different illumination conditions. Reproduced with permission from Ref. [83]. Copyright 2018, Wiley-VCH Verlag GmbH & Co. KGaA, Weinheim.

stimulations, as shown in Fig. 4(b) (Fig. 4(c)). It was believed that the PPC effect in the MoS_2/Si synaptic device was induced by defects (e.g., sulphur vacancies) in MoS_2 and those at the MoS_2/Si interface. The trapping and detrapping of electrons at defects at the MoS_2/Si interface were mainly responsible for the electrical-stimulation-induced resistive switching.

For the W/n-MoS_2/p-Si device, the existence of a native SiO_2 layer with trap sites played a key role in the photoelectric memory. This should enlighten the development of hybrid synaptic devices based on Si. To take advantage of the interfacial traps, ultrathin materials, e.g., monolayer 2D materials, are good candidates to build heterostructures. Surface traps of Si also promise to play a significant role in synaptic devices when the size of Si is reduced into the nanoscale regime.

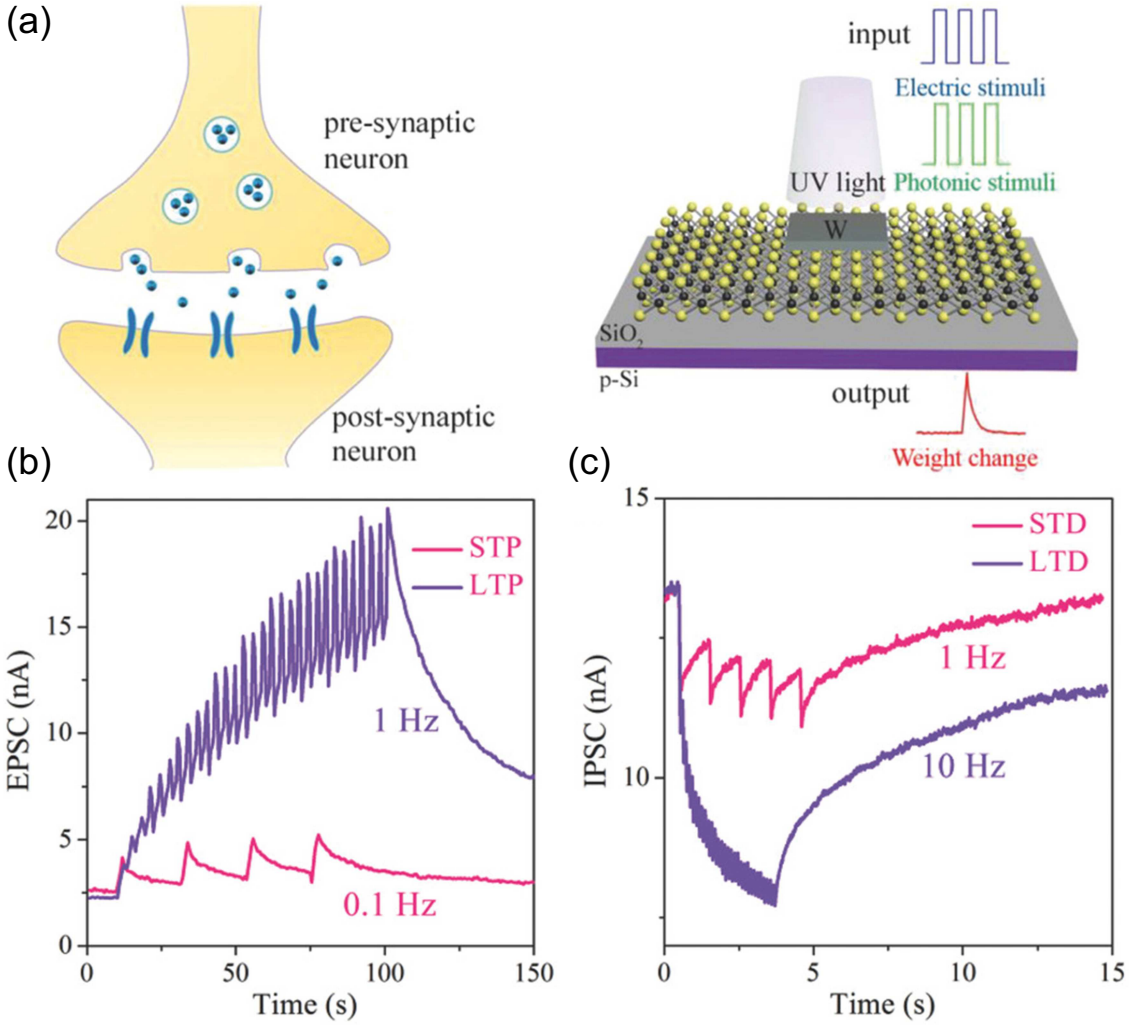


Fig. 4. (a) Schematic of a biological synapse and an optoelectronic synaptic device based on monolayer MoS_2 and bulk Si. (b) Emulation of short-term potentiation and long-term potentiation by using optical spikes. The frequency of the optical spikes was 0.1 Hz or 1 Hz. The power density of the optical spikes was 0.12 mW·cm^{-2}. (c) Emulation of short-term potentiation and long-term potentiation by using −8 V electrical spikes. The frequency of the electrical spikes was 1 Hz or 10 Hz, Reproduced with permission from Ref. [85]. Copyright 2018, Wiley-VCH Verlag GmbH & Co. KGaA, Weinheim.

Given their remarkable optical properties,[86–92] Si nanocrystals (NCs) have recently been used for optically stimulated synaptic devices. Tan *et al.*[93] first proposed two-terminal optoelectronic synaptic devices with the structure of ITO/Si NCs/Al, as illustrated in Fig. 5(a). Si NCs used in these devices were heavily boron doped to enable near-infrared (NIR) light absorption,[94–96] which might facilitate the combination of neuromorphic computing with optical communication.[97] Si NCs worked like vesicles, while holes in Si NCs corresponded to neurotransmitters. Optical stimulations in a broadband wavelength region (375–1870 nm) were used as the presynaptic spikes. As shown in Figs. 5(a)–5(d), basic synaptic functions including EPSC, PPF, and transition from STP to LTP were demonstrated by using these devices. Asymmetric STDP learning rules were also realized by connecting two individual synaptic devices (Figs. 5(e) and 5(a)). The working mechanism of the Si-NC-based synaptic devices was clarified by studying the electronic structure of the Si NCs with scanning tunneling spectroscopy (STS). In-gap states near the conduction band (CB) and band-tail states extending from the valance band (VB) were found (Fig. 5(f)). The in-gap states might be induced by dangling bonds at the Si-NC surface, while the band-tail states could originate from heavy-doping-induced disorder. Figure 5(g) schematically shows the

behavior of photogenerated carriers in the Si NCs. The trapping of photogenerated electrons at the in-gap states and the subsequent slow detrapping through thermal fluctuation were believed to be responsible for the synaptic plasticity of the two-terminal optoelectronic synaptic devices based on Si NCs.

The work of Tan *et al.* expanded the application of Si NCs into optoelectronic synaptic devices for the first time. This was encouraging for the realization of large-scale neuromorphic computing. However, their work failed to emulate the synaptic depression, which could be realized by modifying the device structure or introducing electrical stimuli.[98]

Although optoelectronic synaptic devices often have optical inputs and electrical outputs, Zhao *et al.* have managed to fabricate two-terminal optoelectronic synaptic devices with electrical inputs and optical outputs.[70,71] These devices were fabricated by using light-emitting Si NCs, which could be called Si quantum dots (Si QDs) as well. Figure 6(a) shows the first device structure of ITO/ZnO/Si NCs/CBP/MoO_3/Au. Electroluminescence (EL) at the wavelength of $\sim$ 740 nm was obtained when the devices were stimulated by an electrical spike. The typical change of the EL with time is shown in the inset of Fig. 6(b). The decay time of the EL was around 20 ms, which was in the range (1–10^4 ms) of a typical decay time for signal transmission in a biological synapse. Figure 6(c) illustrates the carrier recombination process in the Si-NC film under a bias voltage. The recombination of the injected holes and electrons gave rise to the EL. During the recombination process, partial injected electrons could be trapped by the deep energy level induced by the dangling bonds at the surface of the Si NCs. The trapped electrons would be detrapped later and tunnel to a neighboring Si NC. In the neighboring Si NC, the recombination between holes and electrons occurred and also generated the EL. The relative long time for the detrapping of electrons resulted in the long EL lifetime.

The Si-NC-based electroluminescent synaptic devices were capable of emulating synaptic plasticity by taking the optical power of the EL as the synaptic weight. Typical PPF was emulated by applying paired electrical spikes (Fig. 6(d)). The transition from STP to LTP was mimicked by changing the quantity (Fig. 6(e)) or frequency (Fig. 6(f)) of consecutive electrical spikes. In the meantime, basic logic functions including AND, OR, NAND, and NOR were also realized by using the Si-NC-based electroluminescent synaptic devices.

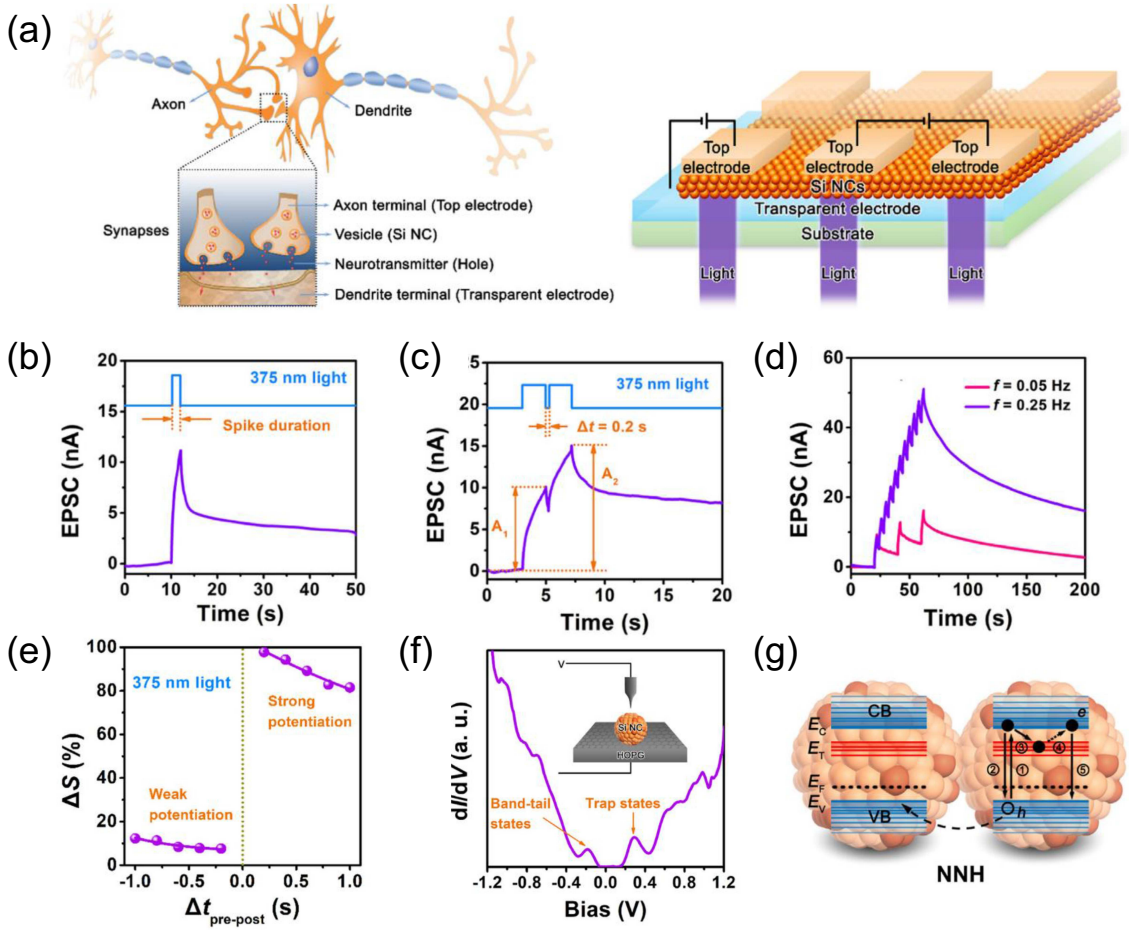


Fig. 5. (a) Schematic of biological synapses and an array of Si-NC-based synaptic devices. (b) EPSC induced by a 375 nm laser spike. (c) PPF behavior induced by two successive 375 nm laser spikes. (d) Transition from STP to LTP by 375 nm laser spiking at the frequencies of 0.05 Hz and 0.25 Hz. (e) Variation of the STDP-induced synaptic-weight change (ΔS) with respect to $\Delta t_{\text{pre-post}}$ for the 375 nm laser spiking. $\Delta t_{\text{pre-post}}$ is the interval time of two identical laser spikes applied to the presynaptic and postsynaptic neurons. (f) The STS result for the Si-NC film measured at 77 K. The inset schematically shows the STS measurement. (g) Schematic model for the electronic structure and carrier behavior of Si NCs. Reproduced with permission from Ref. [93]. Copyright 2018, Elsevier Ltd.

Zhao *et al.*[71] subsequently reported the second device structure of glass/ITO/PEDOT:PSS/P_3HT/PFN/Si-QDs /ZnO/Ag for the Si-NC-based electroluminescent synaptic devices. Figure 7(a) schematically shows this device structure. The flat-band energy-level diagram of this device structure is shown in Fig. 7(b). P3HT was used as the hole-transport layer (HTL), while the ZnO-NC film worked as the electron-transport layer (ETL). A better balance of the carrier injection was obtained because the hole mobility of P3HT was comparable to the electron mobility of the ZnO-NC film. To mitigate the electron leakage from the Si-NC layer toward the anode, an interlayer of PFN was added between P3HT and the Si-NC layer. Figure 7(c) shows the comparison of the power efficiency among the devices with the traditional HTL of poly-TPD, the HTL of P3HT, and the layer of P3HT/PFN. The device with the layer of P3HT/PFN exhibited the highest power efficiency of 4.4%, indicating the most significant reduction of energy consumption. Upon stimulation of an electrical spike,

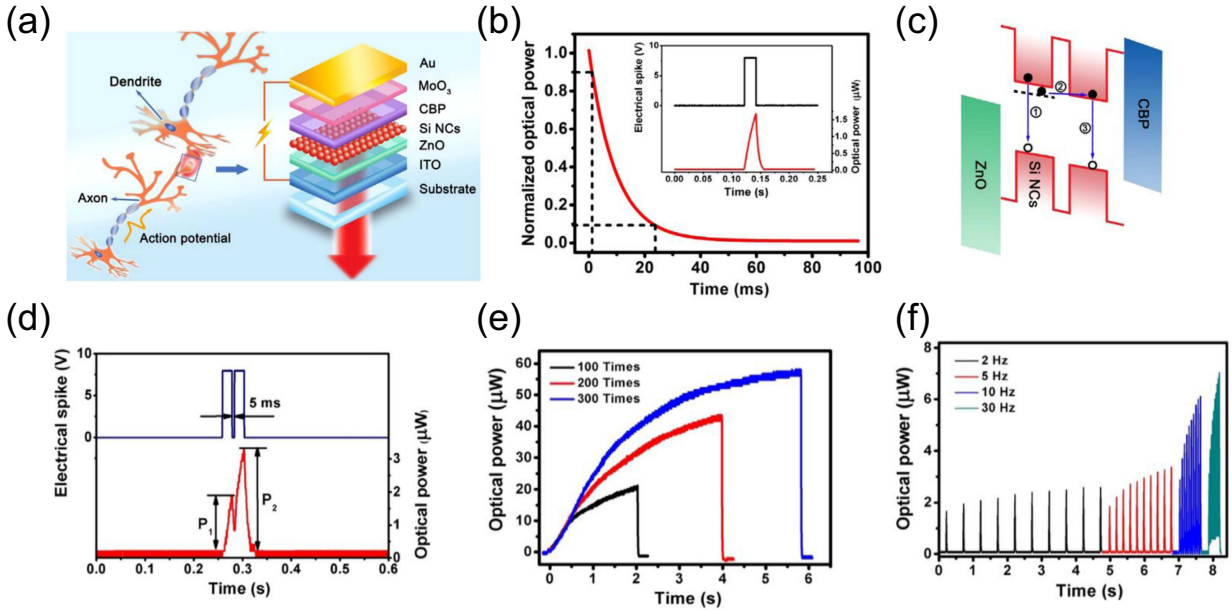


Fig. 6. (a) Schematic of biological neurons and the electroluminescent synaptic device. (b) EL decay of the synaptic device stimulated by an 8 V electrical spike. The inset is the electrical spike and the corresponding optical power of the EL. (c) Band alignment between the ZnO, Si NCs, and CPB layers under a bias voltage. The dangling-bond-induced deep energy level is indicated by the dashed line. (d) PPF induced by two successive electrical spikes with the interval (Δt) of 5 ms. (e) Optical power of the synaptic device stimulated by 8 V electrical spikes, the number of which changes from 100 to 300. (f) Optical power of the synaptic device under the stimulation of ten successive electrical spikes at the spiking frequencies from 2 Hz to 30 Hz. Reproduced with permission from Ref. [70]. Copyright 2018, Elsevier Ltd.

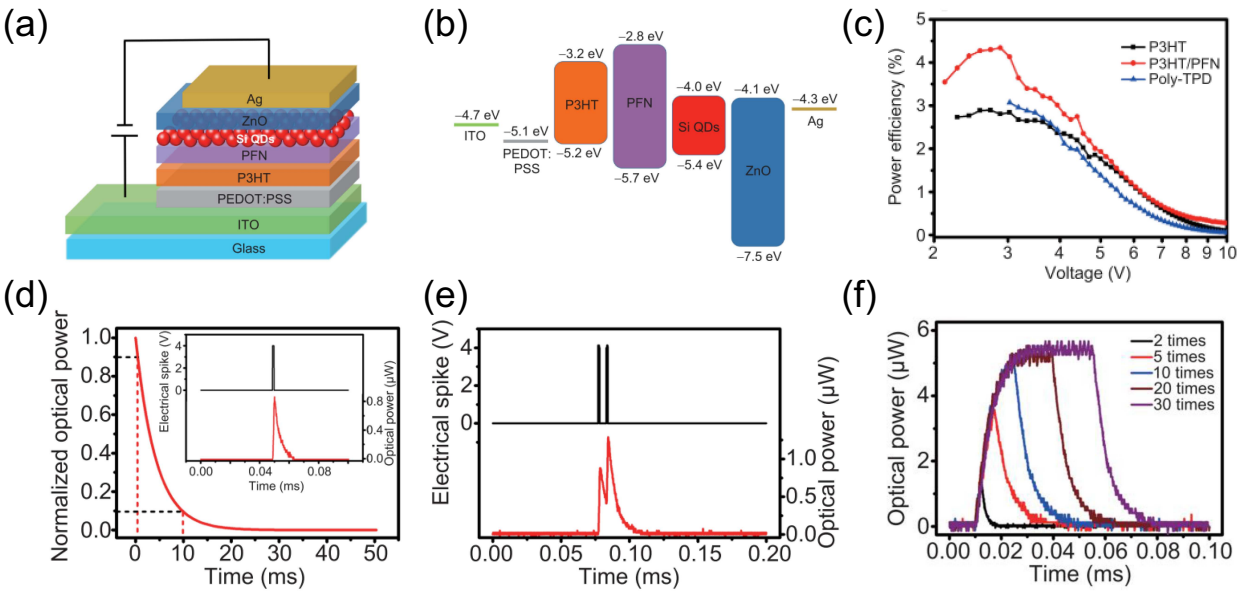


Fig. 7. (a) Schematic diagram and (b) flat-band energy-level diagram of a NIR QLED based on Si QDs with a PFN interlayer. (c) Power efficiency versus voltage for NIR QLEDs based on Si QDs with P3HT, P3HT/PFN, and poly-TPD. (d) Decay of the EL stimulated by a 4 V electrical spike. The inset shows the electrical spike and the corresponding optical power of the EL. (e) PPF induced by two successive electrical spikes. (f) Optical power of a synaptic device stimulated by two to thirty 4 V electrical spikes. Reproduced with permission from Ref. [71]. Copyright 2019, Science China Press and Springer-Verlag GmbH Germany, part of Springer Nature.

a typical device with the layer of P3HT/PFN showed a slow decay time (∼ 10 ms) of the EL at the wavelength of 850 nm (Fig. 7(d)). The PPF and the transition from STP to LTP were also readily demonstrated with the device (Figs. 7(e) and 7(f)).

The Si-NC-based electroluminescent synaptic devices successfully output optical signals with the wavelength of 850 nm. Since the NIR light is vital in nowadays optical communication, the output of NIR light is intriguing for synaptic devices. The realization of electroluminescent synaptic devices may facilitate the bidirectional conversion between optical and electrical signals, which is a critical step in optoelectronic integration of ANNs.

3.2. Three-terminal synaptic devices

Yin *et al.*[99] developed synaptic phototransistors by using boron-doped Si NCs as the channel. The schematic structure of the synaptic Si-NC phototransistors is shown in Fig. 8(a). The Si-NC phototransistors could be stimulated both optically and electrically from the top and backgate, respectively. With the stimulation of an optical spike, IPSC was generated due to photogating (Fig. 8(b)). The photogating was induced by the photo-assisted oxygen desorption at the surface of the Si NCs. Oxygen molecules absorbed at the surface of the Si NCs raised a negative surface potential and upward bent the band structure at the surface. Hence, the photo-generated holes tended to migrate to the near-surface region of the Si NCs, neutralizing oxygen ions and desorbing oxygen molecules. This type of hole scavenging made the conductivity of the Si-NC film decrease. With the stimulation of a negative (positive) electrical spike, IPSC (EPSC) was emulated with a repolarization-hyperpolarization-depolarization behavior (Fig. 8(c)). The unusual behavior of the synaptic Si-NC phototransistors originated from the surface donor (acceptor) states of the gate oxide, well mimicking to that of biological synapses.[58,100]

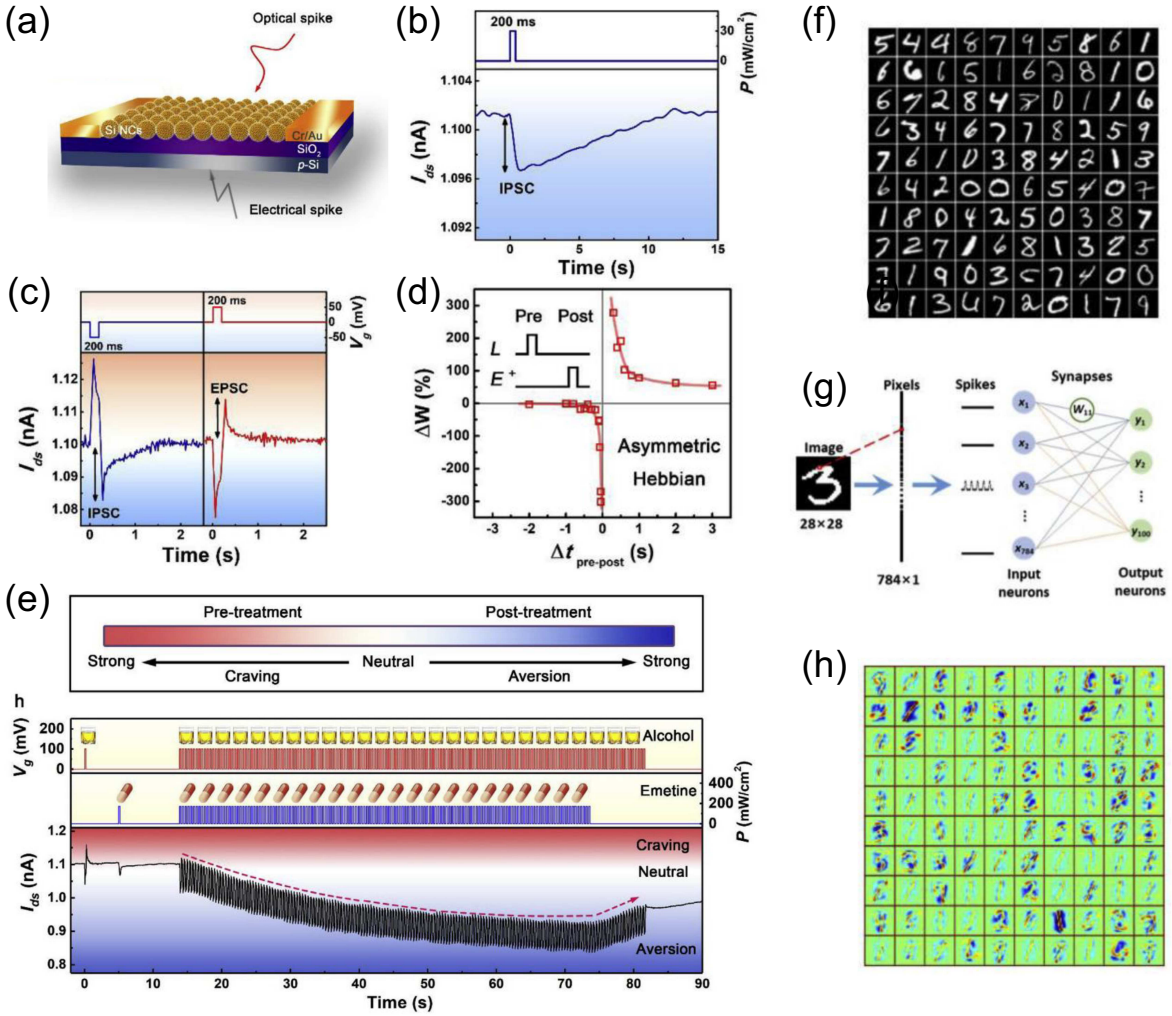


Fig. 8. (a) Schematic of a synaptic Si-NC phototransistor. (b) IPSC induced by a 1342 nm laser spike. (c) IPSC (EPSC) induced by a −50 mV (+50 mV) electrical spike. (d) Dependence of the STDP-induced synaptic weight change (ΔW) on the interval time between the presynaptic and postsynaptic spikes ($\Delta t_{\text{pre-post}}$). ΔW is calculated by using $\Delta W = \Delta\text{PSC/PSC1}$, where ΔPSC results from the subtraction of the postsynaptic current of the first spike (PSC1) from that of the last spike. (e) Implementation of taste aversion learning with a synaptic Si-NC phototransistor. (f) Example images in the MNIST database after the binarization with a pixel threshold of 50. (g) The architecture of the SNN. (h) Receptive fields of all output neurons in the network. Reproduced with permission from Ref. [99]. Copyright 2019, Elsevier Ltd.

With the stimulation of combined optical spikes, negative electrical spikes, and positive electrical spikes, symmetric/asymmetric Hebbian/anti-Hebbian STDP learning rules were realized by the synaptic Si-NC phototransistors. Figure 8(d) shows the asymmetric Hebbian STDP learning rule realized by using an optical spike (L) and a positive electrical spike (E^+). Aversion learning, which is a type of associative learning, was also implemented by the synaptic Si-NC phototransistors. Figure 8(e) illustrates the taste aversion learning process. An EPSC triggered by a positive electrical spike was regarded as the craving for alcohol, while an IPSC triggered by an optical spike was regarded as the aversion for alcohol. The situation that a patient with alcoholism gained aversion for alcohol after the aversion learning was well simulated. Here the positive electrical spike was taken as drinking alcohol while the optical spike was viewed as methods of treating alcoholism, e.g. inducing emesis by taking emetine. With repeatedly electrical and optical stimulations, the current of the device turned very low. This resembled the aversion to alcohol of the patient induced by repeatedly drinking alcohol and taking emetine. A spiking neural network (SNN) was further simulated by forming a crossbar array of a synaptic weight layer with the Si-NC phototransistors. Tasks of recognizing the handwritten digits were executed by the SNN. Figure 8(f) shows binarized handwritten digit images derived from handwritten digits in the modified National Institute of Standards and Technology (MNIST) database. These images were input into a spiking neural network (Fig. 8(g)), which were based on 784 input neurons and 100 output neurons. It turned out that the images might be recognized by the SNN with an accuracy of $\sim 93\%$. Figure 8(h) shows the corresponding receptive fields of the output neurons after the training.

Feasible energy consumption is still a major obstacle for nowadays hardware-based ANNs to compete with the biological neural systems.[28] Although augmentative functionalities can be realized by the synaptic Si-NC phototransistors, the energy consumption (~ 10 nJ) of the device is much higher than that of a human brain (tens of fJ).[101] Ni *et al.*[102] demonstrated synaptic phototransistors based on the hybrid structure of 2D WSe_2 and Si NCs (Fig. 9(a)). These devices were very sensitive to optical stimulation. An optical spike with the energy of ~ 75 fJ might trigger the response of the devices with the device area of 300 μm^2. It was proposed that the 2D WSe_2 was depleted by the Si NCs after the hybrid structure was formed, enhancing the optical sensitivity of the devices. Figure 9(b) shows the transfer curves of the 2D WSe_2-based transistor and the Si-NC/WSe_2-based transistor. A left shift could be observed after the incorporation of Si NCs. With positive gate voltage, the drain current of the Si-NC/WSe_2-based transistor was lower than that of the 2D WSe_2-based transistor. Hence the 2D WSe_2 was depleted by the Si NCs, which could be further evidenced by the band alignment between Si NCs and 2DWSe_2 (the inset of Fig. 9(b)).

Synaptic phototransistors based on Si NCs facilitated the development of energy-efficient neuromorphic computing. Studies on Si-based three-terminal synaptic devices are ongoing these days. Inspired by phototransistors based on Si NCs, efforts can be also devoted to synaptic transistors based on other Si nanostructures. Given the broad applications of Si and the existing CMOS technology, the fabrication process of ANNs may be simplified in the future.

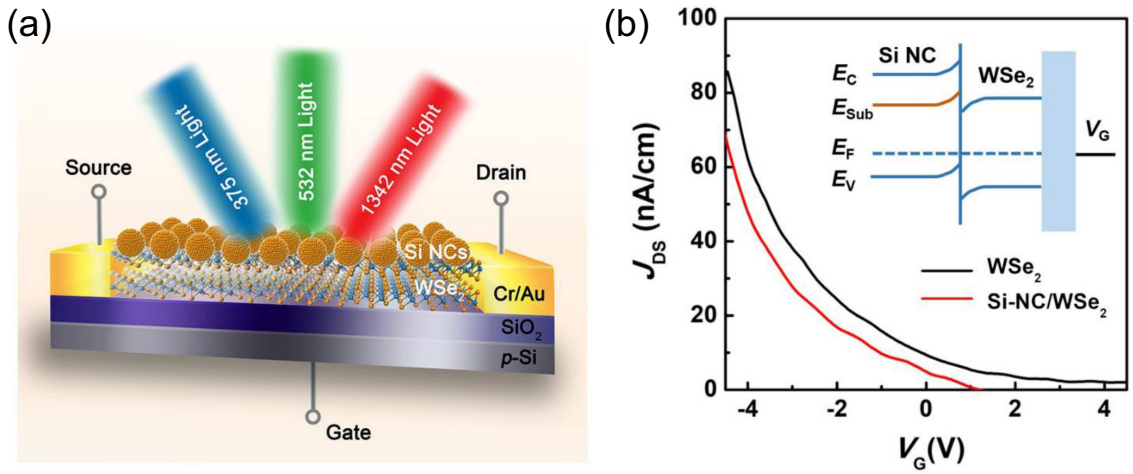


Fig. 9. (a) Schematic of the Si-NC/WSe_2 synaptic device structure. (b) Transfer curves of WSe_2 and Si-NC/WSe_2 TFTs. The inset shows the band alignment between Si NCs and WSe_2. Reproduced with permission from Ref. [102]. Copyright 2018, IEEE.

4. Remarks and outlook

Neuromorphic computing, which is an emerging computing paradigm, has gained numerous attention ever since the 1980s for its potential in artificial intelligence.[103] Inspired by biological neural networks, there have been a variety of ANNs including convolutional neural networks, recurrent neural networks, and SNNs. Hardware implementation of these ANNs is mainly based on CMOS integrated circuits, as evidenced by the IBM's TrueNorth[104] and the Intel's Loihi.[105] In recent years, memristors have been extensively studied for the devel-

opment of electronic ANNs.[106,107] Research on optoelectronically integrated artificial networks is now in the early stage. Farhat *et al.*[108] proposed an optoelectronic neural network in 1985. The neural network was based on the Hopfield model. In the network, a light-emitting diode (LED) array was used to supply the input vector of light signals. An array of photodiodes was used to detect the output vector and convert the optical signals to electrical signals. The synaptic weight was controlled by the optical power which could be programmed through a shadow mask of metal, imaged mask, light valve, or raster-scanned laser beam.[109] The principle of a-Si:H based neural networks was similar. The a-Si:H synaptic devices were only used as the photoconductors to realize a matrix multiplier.

The optoelectronic ANNs proposed by Farhat *et al.* are far from current demands in terms of complexity, scalability, and energy-efficiency. Intriguing efforts have been recently focused on using synaptic devices to emulate the retina of the biological visual system. The retina is capable of optical sensing, data storage, and real-time processing. Novel optoelectronic synaptic devices with proper sensing-memory-processing functions are booming with diverse materials and device structures. In this context, Si is playing a critical role. For example, in the Pt/HfO_2/Si device Si was not only the photoreceptor but also the intermediary agent modulating the device resistance. In the Si NCs-based devices, the dangling bonds or absorbed oxygen molecules at the Si-NC surface were utilized to realize the synaptic plasticity. In the W/n-MoS_2/p-Si device, the native oxide on Si substrate supplied trap sites for both the photogenerated and electrically injected carriers.

Please note that working mechanism varied among these Si-based devices. The Pt/HfO_2/Si device realized nonvolatile memory behavior by using the HfO_2, which was one of the mature metal oxides used in oxygen-filament-based memristors. With the change of the voltage drop on the HfO_2, the resistance of the device could be regulated. The nonvolatile memory with multiple analog states was desired for current ANN frameworks, e.g., hardware-based convolutional neural networks[110,111] and recurrent neural networks.[112] In such networks, the synaptic weights are directly programmed to the conductance of the synaptic devices. The conductance of the synaptic devices should be kept with a long retention time so that the synaptic weights could be maintained before the next update. With optoelectronic spikes the Pt/HfO_2/Si device could also exhibit STDP-like characteristics, which were required for the implementation of the next-generation SNNs. Strictly speaking, the Pt/HfO_2/Si device was only electrically stimulated with the assistance of light. Further work is need to enable the optical stimulation for the Pt/HfO_2/Si device.

In the W/n-MoS_2/p-Si and ITO/Si NCs/Al devices, volatile memory with the retention time of dozens of seconds was induced by the charge trapping/detrapping. The Si-NC-based electroluminescent devices also exhibited volatile memory with the retention time of milliseconds due to the charge trapping/detrapping. Although the retention time in these devices could be tuned by the parameters of the optical stimulation, the retention time significantly differed among the devices. We would like to mention that an optimal retention time is hard to define at this moment. Biologically, STP usually lasts from several milliseconds to minutes, while LTP can last for several hours or days. In an ANN, the required spatiotemporal dynamics may not be exactly the same as that of a biological neural network. The retention time for synaptic devices is intimately related to neuromorphic algorithms and architectures for a specific application scenario.[113] The working mechanism of charge trapping/detrapping has been widely used in optoelectronic synaptic devices although the role of traps has not been completely clarified nowadays. Traps are usually avoided in photodetectors and solar cells in order to maximize the photoelectric conversion efficiency. However, for synaptic devices, traps can help emulate the synaptic plasticity. We should note that traps may lead to device variation. However, it seems that an ANN may well tolerate the device variation.[114]

Different from the Si-NC-based two-terminal devices, the synaptic Si-NC phototransistors could emulate IPSC by taking advantage of photogating. It is usually hard to emulate the synaptic depression for optoelectronic synaptic devices. Electrical spikes are normally used for the emulation of synaptic depression.[32,115] Photogating induced negative photoconductance has been observed in several nanostructures such as carbon nanotubes,[116] ZnSe nanowires,[117] and InAs nanowires.[118] Inspired by the synaptic Si-NC phototransistors, employing these devices with negative photoconductance to realize the synaptic depression may be a promising approach. Researches on Si-NC-based synaptic devices have demonstrated the superiority of nanomaterials for the fabrication of synaptic devices. In the past decades, methods of tuning the surface, size, and doping have been developed for Si NCs, which rendered Si NCs diverse optical and electrical properties.[119] This facilitated the exploration of Si NCs for optoelectronic synapses. Please note that the optical and electrical properties of other Si nanostructures such as Si nanowires,[120] Si nanosheets,[121] and Si nanomembranes[122] also strongly depend on the surface/interfacial traps. Investigation on the use of these Si nanostructures for the fabrication of optoelectronic synaptic devices should be interesting as well.

Optoelectronic synaptic devices usually have two-terminal or three-terminal structures. When integrated into a network, the two-terminal synaptic devices form a crossbar array. The simplicity of such an array can ensure high-density

integration. However, it is still challenging for the use of two-terminal synaptic devices in artificial vision systems. On one hand, it is difficult for the two-terminal devices to realize a nondestructive weight update because the electrical reading and writing operations are done by one shared terminal.[77,123] On the other hand, the coexistence of electro- and photo-active functionalities in a single material that is usually used for a two-terminal device rarely occurs.[38,72] On the contrary, the three-terminal synaptic devices (e.g., synaptic transistors) can incorporate augmentative functionalities by accommodating versatile control parameters.[124,125] Gate dielectric or photogating effect can be utilized to modulate the electronic properties, facilitating the combination of the physical properties of different assembled elements in an individual structure.[29,126] Moreover, multiple gates can be used for a synaptic transistor, which can emulate the spatial summation of postsynaptic current in a biological neural network.[3,127,128] Therefore, the three-terminal synaptic devices are more appealing for the hardware-based neuromorphic computing despite the relatively high circuit complexity.

Biological synapses operate at extremely low energy levels with the energy consumption of $\sim$ 20 fJ per event.[129] However, energy consumption of synaptic devices remains rather high up to now.[28] For an optoelectronic synaptic device, the energy consumption consists of the electrical and optical components. The electrical energy consumption can be calculated by using the integration of UI over time, where U and I are the voltage and current across the device, respectively. The optical energy is determined by the light source, which can be natural or artificial depending on the application scenarios. In fact, the optical energy may be also used to evaluate the optical sensitivity of the device. To minimize the energy consumption, the choice of materials and device structures for synaptic devices is critical.

Although the potential of Si-based optoelectronic synaptic devices for neuromorphic computing has been well witnessed, more efforts are definitely needed to devote to the development of highly intelligent and energy-efficient Si-based optoelectronic synaptic devices. In the meantime, the achievements of Si photonics[130] should be exploited to incorporate Si-based optoelectronic synaptic devices into ANNs.

5. Conclusion

We have presented advances in Si-based optoelectronic synaptic devices. Amorphous Si, bulk Si, and Si NCs have been used in optoelectronic synaptic devices. This should encourage the exploration of other Si materials for the fabrication of optoelectronic synaptic devices. Although the two-terminal and three-terminal device structures are popular for Si-based optoelectronic synaptic devices, novel device structures deserve investigation in the context of optoelectronic integration for ANNs. One of the direct applications of Si-based optoelectronic synaptic devices is for the simulation of a visual neural system. Further improvement of the synaptic functionalities and further reduction of the energy consumption for Si-based optoelectronic synaptic devices will greatly contribute to the realization of the visual neural system based on these devices.

References

[1] Waldrop M M 2012 *Nature* **482** 456
[2] Zidan M A, Strachan J P and Lu W D 2018 *Nat. Electron.* **1** 22
[3] Bear M F, Connors B W and Paradiso M A 2007 *Neuroscience: Exploring the Brain, Enhanced Edition* Vol. **2** (Jones & Bartlett Learning, LLC)
[4] Drachman D A 2005 *Neurology* **64** 2004
[5] Abbott L F and Regehr W G 2004 *Nature* **431** 796
[6] Akopyan F, Sawada J, Cassidy A, Alvarez-Icaza R, Arthur J, Merolla P, Imam N, Nakamura Y, Datta P, Nam G J, Taba B, Beakes M, Brezzo B, Kuang J B, Manohar R, Risk W P, Jackson B and Modha D S 2015 *IEEE Trans. Comput. Des. Integr. Circuits Syst.* **34** 1537
[7] Poon C S and Zhou K 2011 *Front. Neurosci.* **5** 2009
[8] Chicca E, Stefanini F, Bartolozzi C and Indiveri G 2014 *Proc. IEEE* **102** 1367
[9] Rahimi Azghadi M, Iannella N, Al-Sarawi S F, Indiveri G and Abbott D 2014 *Proc. IEEE* **102** 717
[10] Indiveri G, Chicca E and Douglas R 2006 *IEEE Trans. Neural Networks* **17** 211
[11] Wijekoon J H B and Dudek P 2008 *Neural Networks* **21** 524
[12] Rahimi Azghadi M, Al-Sarawi S, Abbott D and Iannella N 2013 *Neural Networks* **45** 70
[13] Kuzum D, Yu S and Philip Wong H S 2013 *Nanotechnology* **24** 382001
[14] Kim C H, Lim S, Woo S Y, Kang W M, Seo Y T, Lee S T, Lee S, Kwon D, Oh S, Noh Y, Kim H, Kim J, Bae J H and Lee J H 2019 *Nanotechnology* **30** 032001
[15] Islam R, Li H, Chen P Y, Wan W, Chen H Y, Gao B, Wu H, Yu S, Saraswat K and Philip Wong H S 2019 *J. Phys. D: Appl. Phys.* **52** 113001
[16] Tang J, Yuan F, Shen X, Wang Z, Rao M, He Y, Sun Y, Li X, Zhang W, Li Y, Gao B, Qian H, Bi G, Song S, Yang J J and Wu H 2019 *Adv. Mater.* **31** 1902761
[17] Tian H, Zhao L, Wang X, Yeh Y W, Yao N, Rand B P and Ren T L 2017 *ACS Nano* **11** 12247
[18] Yan X B, Zhao J H, Liu S, Zhou Z Y, Liu Q, Chen J S and Liu X Y 2018 *Adv. Funct. Mater.* **28** 1
[19] Hu L, Fu S, Chen Y, Cao H, Liang L, Zhang H, Gao J, Wang J and Zhuge F 2017 *Adv. Mater.* **29** 1606927
[20] Benner A F, Ignatowski M, Kash J A, Kuchta D M and Ritter M B 2005 *IBM J. Res. Dev.* **49** 755
[21] Wang Z, Zhang S, Zhou L, Mao J, Han S, Ren Y, Yang J, Wang Y, Zhai Y and Zhou Y 2019 *Phys. Status Solidi - Rapid Res. Lett.* **13** 1800644
[22] Han H, Yu H, Wei H, Gong J and Xu W 2019 *Small* **15** 1900695
[23] Lee M, Lee W, Choi S, Jo J W, Kim J, Park S K and Kim Y H 2017 *Adv. Mater.* **29** 1700951
[24] John R A, Liu F, Chien N A, Kulkarni M R, Zhu C, Fu Q, Basu A, Liu Z and Mathews N 2018 *Adv. Mater.* **30** e1800220
[25] Ham S, Choi S, Cho H, Na S I and Wang G 2019 *Adv. Funct. Mater.* **29** 1806646
[26] Kumar M, Kim H S and Kim J 2019 *Adv. Mater.* **31** 1900021
[27] Sun F, Lu Q, Liu L, Li L, Wang Y, Hao M, Cao Z, Wang Z, Wang S, Li T and Zhang T 2020 *Adv. Mater. Technol.* **5** 1900888
[28] Yu J J, Liang L Y, Hu L X, Duan H X, Wu W H, Zhang H L, Gao J H, Zhuge F, Chang T C and Cao H T 2019 *Nano Energy* **62** 772
[29] He W, Fang Y, Yang H, Wu X, He L, Chen H and Guo T 2019 *J. Mater. Chem. C* **7** 12523
[30] Seo S, Jo S H, Kim S, Shim J, Oh S, Kim J H, Heo K, Choi J W, Choi C, Oh S, Kuzum D, Wong H S P and Park J H 2018 *Nat. Commun.* **9** 5106
[31] Zhao L, Fan Z, Cheng S, Hong L, Li Y, Tian G, Chen D, Hou Z, Qin M, Zeng M, Lu X, Zhou G, Gao X and Liu J 2020 *Adv. Electron. Mater.* **6** 1900858

[32] Hu D C, Yang R, Jiang L and Guo X 2018 *ACS Appl. Mater. Interfaces* **10** 6463
[33] Li H K, Chen T P, Liu P, Hu S G, Liu Y, Zhang Q and Lee P S 2016 *J. Appl. Phys.* **119** 244505
[34] Duan N, Li Y, Chiang H C, Chen J, Pan W Q, Zhou Y X, Chien Y C, He Y H, Xue K H, Liu G, Chang T C and Miao X S 2019 *Nanoscale* **11** 17590
[35] Kumar M, Abbas S and Kim J 2018 *ACS Appl. Mater. Interfaces* **10** 34370
[36] Guo Y B, Zhu L Q, Gao W T, Ren Z Y, Xiao H and Ge Z Y 2019 *Org. Electron.* **71** 31
[37] Peng C, Jiang W, Li Y, Li X and Zhang J 2019 *ACS Appl. Electron. Mater.* **1** 2406
[38] Gao S, Liu G, Yang H, Hu C, Chen Q, Gong G, Xue W, Yi X, Shang J and Li R W 2019 *ACS Nano* **13** 2634
[39] Pilarczyk K, Podborska A, Lis M, Kawa M, Migdal D and Szaciłowski K 2016 *Adv. Electron. Mater.* **2** 1500471
[40] Liu Z, Dai S, Wang Y, Yang B, Hao D, Liu D, Zhao Y, Fang L, Ou Q, Jin S, Zhao J and Huang J 2020 *Adv. Funct. Mater.* **30** 1906335
[41] Qin S, Wang F, Liu Y, Wan Q, Wang X, Xu Y, Shi Y, Wang X and Zhang R 2016 *2D Mater.* **4** 035022
[42] Shao L, Wang H, Yang Y, He Y, Tang Y, Fang H, Zhao J, Xiao H, Liang K, Wei M, Xu W, Luo M, Wan Q, Hu W, Gao T and Cui Z 2019 *ACS Appl. Mater. Interfaces* **11** 12161
[43] Zhu X and Lu W D 2018 *ACS Nano* **12** 1242
[44] Qian L, Sun Y, Wu M, Li C, Xie D, Ding L and Shi G 2018 *Nanoscale* **10** 6837
[45] Sun Y, Qian L, Xie D, Lin Y, Sun M, Li W, Ding L, Ren T and Palacios T 2019 *Adv. Funct. Mater.* **29** 1902538
[46] Tian H, Wang X, Wu F, Yang Y and Ren T L 2018 *2018 IEEE International Electron Devices Meeting (IEDM)* vol. 2018-Decem (IEEE) pp. 38.6.1–38.6.4
[47] Wang Y, Lv Z, Chen J, Wang Z, Zhou Y, Zhou L, Chen X and Han S T 2018 *Adv. Mater.* **30** 1802883
[48] Wang K, Dai S, Zhao Y, Wang Y, Liu C and Huang J 2019 *Small* **15** 1900010
[49] John R A, Liu F, Chien N A, Kulkarni M R, Zhu C, Fu Q, Basu A, Liu Z and Mathews N 2018 *Adv. Mater.* **30** 1800220
[50] Wang S, Chen C, Yu Z, He Y, Chen X, Wan Q, Shi Y, Zhang D W, Zhou H, Wang X and Zhou P 2019 *Adv. Mater.* **31** 1806227
[51] Zhou F, Chen J, Tao X, Wang X and Chai Y 2019 *Research* **2019** 9490413
[52] Luo Z D, Xia X, Yang M M, Wilson N R, Gruverman A and Alexe M 2020 *ACS Nano* **14** 746
[53] Wang S, Hou X, Liu L, Li J, Shan Y, Wu S, Zhang D W and Zhou P 2019 *Research* **2019** 1618798
[54] Kim S G, Kim S H, Park J, Kim G S, Park J H, Saraswat K C, Kim J and Yu H Y 2019 *ACS Nano* **13** 10294
[55] Zuo F, Panda P, Kotiuga M, Li J, Kang M, Mazzoli C, Zhou H, Barbour A, Wilkins S, Narayanan B, Cherukara M, Zhang Z, Sankaranarayanan S K R S, Comin R, Rabe K M, Roy K and Ramanathan S 2017 *Nat. Commun.* **8** 240
[56] Efros A L, Delehanty J B, Huston A L, Medintz I L, Barbic M and Harris T D 2018 *Nat. Nanotechnol.* **13** 278
[57] Zucker R S and Regehr W G 2002 *Annu. Rev. Physiol.* **64** 355
[58] Ferster D and Jagadeesh B 1992 *J. Neurosci.* **12** 1262
[59] Salin P A, Scanziani M, Malenka R C and Nicoll R A 1996 *Proc. Natl. Acad. Sci. USA* **93** 13304
[60] Lin Y, Zeng T, Xu H, Wang Z, Zhao X, Liu W, Ma J and Liu Y 2018 *Adv. Electron. Mater.* **4** 1800373
[61] Zhou L, Yang S, Ding G, Yang J Q, Ren Y, Zhang S R, Mao J Y, Yang Y, Zhou Y and Han S T 2019 *Nano Energy* **58** 293
[62] Kirkwood A, Dudek S M, Gold J T, Aizenman C D and Bear M F 1993 *Science* **260** 1518
[63] Feldman D E 2012 *Neuron* **75** 556
[64] Xiao Z and Huang J 2016 *Adv. Electron. Mater.* **2** 1600100
[65] Ren Y, Hu L, Mao J Y, Yuan J, Zeng Y J, Ruan S, Yang J Q, Zhou L, Zhou Y and Han S T 2018 *J. Mater. Chem. C* **6** 9383
[66] Citri A and Malenka R C 2008 *Neuropsychopharmacology* **33** 18
[67] Dudek S M and Bear M F 1992 *Proc. Natl. Acad. Sci. USA* **89** 4363
[68] Aizenman C D, Manis P B and Linden D J 1998 *Neuron* **21** 827
[69] Yu F, Zhu L Q, Xiao H, Gao W T and Guo Y B 2018 *Adv. Funct. Mater.* **28** 1804025
[70] Zhao S, Ni Z, Tan H, Wang Y, Jin H, Nie T, Xu M, Pi X and Yang D 2018 *Nano Energy* **54** 383
[71] Zhao S, Wang Y, Huang W, Jin H, Huang P, Wang H, Wang K, Li D, Xu M, Yang D and Pi X 2019 *Sci. China Mater.* **62** 1470
[72] Josberger E E, Deng Y, Sun W, Kautz R and Rolandi M 2014 *Adv. Mater.* **26** 4986
[73] Zhou F, Zhou Z, Chen J, Choy T H, Wang J, Zhang N, Lin Z, Yu S, Kang J, Wong H S P and Chai Y 2019 *Nat. Nanotechnol.* **14** 776
[74] Qian C, Oh S, Choi Y, Kim J H, Sun J, Huang H, Yang J, Gao Y, Park J H and Cho J H 2019 *Nano Energy* **66** 104095
[75] Sun J, Oh S, Choi Y, Seo S, Oh M J, Lee M, Lee W B, Yoo P J, Cho J H and Park J H 2018 *Adv. Funct. Mater.* **28** 1804397
[76] Fang L, Dai S, Zhao Y, Liu D and Huang J 2020 *Adv. Electron. Mater.* **6** 1901217
[77] Boybat I, Le Gallo M, Nandakumar S R, Moraitis T, Parnell T, Tuma T, Rajendran B, Leblebici Y, Sebastian A and Eleftheriou E 2018 *Nat. Commun.* **9** 2514
[78] Ohno T, Hasegawa T, Tsuruoka T, Terabe K, Gimzewski J K and Aono M 2011 *Nat. Mater.* **10** 591
[79] Rietman E A, Frye R C, Wong C C and Kornfeld C D 1989 *Appl. Opt.* **28** 3474
[80] Frye R C, Rietman E A, Wong C C and Chin B L 1989 *International Joint Conference on Neural Networks (IEEE)* pp. 457–63 vol. 2
[81] Frye R C, Rietman E A and Wong C C 1991 *IEEE Trans. Neural Networks* **2** 110
[82] Rietman E A, Frye R C and Wong C C 1991 *Appl. Opt.* **30** 950
[83] Chen Y, Wei Q, Yin J, Xia Y and Liu Z 2018 *Adv. Electron. Mater.* **4** 1800242
[84] John R A, Yantara N, Ng Y F, Narasimman G, Mosconi E, Meggiolaro D, Kulkarni M R, Gopalakrishnan P K, Nguyen C A, De Angelis F, Mhaisalkar S G, Basu A and Mathews N 2018 *Adv. Mater.* **30** 1805454
[85] He H K, Yang R, Zhou W, Huang H M, Xiong J, Gan L, Zhai T Y and Guo X 2018 *Small* **14** 1800079
[86] Hessel C M, Reid D, Panthani M G, Rasch M R, Goodfellow B W, Wei J, Fujii H, Akhavan V and Korgel B A 2012 *Chem. Mater.* **24** 393
[87] Kortshagen U R, Sankaran R M, Pereira R N, Girshick S L, Wu J J and Aydil E S 2016 *Chem. Rev.* **116** 11061
[88] Clark R J, Aghajamali M, Gonzalez C M, Hadidi L, Islam M A, Javadi M, Mobarok M H, Purkait T K, Robidillo C J T, Sinelnikov R, Thiessen A N, Washington J, Yu H and Veinot J G C 2017 *Chem. Mater.* **29** 80
[89] Sychugov I, Valenta J and Linnros J 2017 *Nanotechnology* **28** 072002
[90] Fujii M, Sugimoto H and Imakita K 2016 *Nanotechnology* **27** 262001
[91] Rocks C, Svrcek V, Velusamy T, Macias-Montero M, Maguire P and Mariotti D 2018 *Nano Energy* **50** 2455
[92] Ray S K, Maikap S, Banerjee W and Das S 2013 *J. Phys. D: Appl. Phys.* **46** 153001
[93] Tan H, Ni Z, Peng W, Du S, Liu X, Zhao S, Li W, Ye Z, Xu M, Xu Y, Pi X and Yang D 2018 *Nano Energy* **52** 422
[94] Ni Z, Ma L, Du S, Xu Y, Yuan M, Fang H, Wang Z, Xu M, Li D, Yang J, Hu W, Pi X and Yang D 2017 *ACS Nano* **11** 9854
[95] Ni Z, Pi X, Zhou S, Nozaki T, Grandidier B and Yang D 2016 *Adv. Opt. Mater.* **4** 700
[96] Zhou S, Ni Z, Ding Y, Sugaya M, Pi X and Nozaki T 2016 *ACS Photonics* **3** 415
[97] Kaushal H and Kaddoum G 2016 *IEEE Commun. Surv. tutorials* **19** 57
[98] Kawauchi T, Kano S and Fujii M 2019 *ACS Appl. Electron. Mater.* **1** 2664
[99] Yin L, Han C, Zhang Q, Ni Z, Zhao S, Wang K, Li D, Xu M, Wu H, Pi X and Yang D 2019 *Nano Energy* **63** 103859
[100] Kamp F, Chen Y and Westerhoff H V 1988 *Biophys. Chem.* **30** 113
[101] Sun L, Zhang Y, Hwang G, Jiang J, Kim D, Eshete Y A, Zhao R and Yang H 2018 *Nano Lett.* **18** 3229
[102] Ni Z, Wang Y, Liu L, Zhao S, Xu Y, Pi X and Yang D 2018 *IEEE International Electron Devices Meeting (IEDM)* (IEEE) pp. 38.5.1–38.5.4
[103] Mead C 1990 *Proc. IEEE* **78** 1629
[104] Merolla P A, Arthur J V., Alvarez-Icaza R, Cassidy A S, Sawada J, Akopyan F, Jackson B L, Imam N, Guo C, Nakamura Y, Brezzo B, Vo I, Esser S K, Appuswamy R, Taba B, Amir A, Flickner M D, Risk W P, Manohar R and Modha D S 2014 *Science* **345** 668

[105] Davies M, Srinivasa N, Lin T H, Chinya G, Cao Y, Choday S H, Dimou G, Joshi P, Imam N, Jain S, Liao Y, Lin C K, Lines A, Liu R, Mathaikutty D, McCoy S, Paul A, Tse J, Venkataramanan G, Weng Y H, Wild A, Yang Y and Wang H 2018 *IEEE Micro* **38** 82
[106] Wang Z, Joshi S, Savel'ev S, Song W, Midya R, Li Y, Rao M, Yan P, Asapu S, Zhuo Y, Jiang H, Lin P, Li C, Yoon J H, Upadhyay N K, Zhang J, Hu M, Strachan J P, Barnell M, Wu Q, Wu H, Williams R S, Xia Q and Yang J J 2018 *Nat. Electron.* **1** 137
[107] Bayat F M, Prezioso M, Chakrabarti B, Nili H, Kataeva I and Strukov D 2018 *Nat. Commun.* **9** 2331
[108] Farhat N H, Psaltis D, Prata A and Paek E 1985 *Appl. Opt.* **24** 1469
[109] Boyd G D 1987 *Appl. Opt.* **26** 2712
[110] Prezioso M, Merrikh-Bayat F, Hoskins B D, Adam G C, Likharev K K and Strukov D B 2015 *Nature* **521** 61
[111] Gokmen T, Onen M and Haensch W 2017 *Front. Neurosci.* **11** 1-13
[112] Li C, Wang Z, Rao M, Belkin D, Song W, Jiang H, Yan P, Li Y, Lin P, Hu M, Ge N, Strachan J P, Barnell M, Wu Q, Williams R S, Yang J J and Xia Q 2019 *Nat. Mach. Intell.* **1** 49-57
[113] Burr G W, Shelby R M, Sebastian A, Kim S, Kim S, Sidler S, Virwani K, Ishii M, Narayanan P, Fumarola A, Sanches L L, Boybat I, Le Gallo M, Moon K, Woo J, Hwang H and Leblebici Y 2017 *Adv. Phys. X* **2** 89-124
[114] Kuzum D, Jeyasingh R G D, Yu S and Wong H S P 2012 *IEEE Trans. Electron Devices* **59** 3489
[115] Ge C, Liu C X, Zhou Q L, Zhang Q H, Du J Y, Li J K, Wang C, Gu L, Yang G Z and Jin K J 2019 *Adv. Mater.* **31** 1900379
[116] Chen R J, Franklin N R, Kong J, Cao J, Tombler T W, Zhang Y and Dai H 2001 *Appl. Phys. Lett.* **79** 2258
[117] Zhang X, Jie J, Wang Z, Wu C, Wang L, Peng Q, Yu Y, Jiang P and Xie C 2011 *J. Mater. Chem.* **21** 6736
[118] Han Y, Zheng X, Fu M, Pan D, Li X, Guo Y, Zhao J and Chen Q 2016 *Phys. Chem. Chem. Phys.* **18** 818
[119] Ni Z, Zhou S, Zhao S, Peng W, Yang D and Pi X 2019 *Mater. Sci. Eng. R Reports* **138** 85
[120] Dan Y 2015 *Appl. Phys. Lett.* **106** 053117
[121] Lu A J, Yang X B and Zhang R Q 2009 *Solid State Commun.* **149** 153
[122] Chen F, Ramayya E B, Euaruksakul C, Himpsel F J, Celler G K, Ding B J, Knezevic I and Lagally M G 2010 *ACS Nano* **4** 2466
[123] Wang Z, Joshi S, Savel'ev S E, Jiang H, Midya R, Lin P, Hu M, Ge N, Strachan J P, Li Z, Wu Q, Barnell M, Li G, Xin H L, Williams R S, Xia Q and Yang J J 2017 *Nat. Mater.* **16** 101
[124] Yang J T, Ge C, Du J Y, Huang H Y, He M, Wang C, Lu H B, Yang G Z and Jin K J 2018 *Adv. Mater.* **30** 1801548
[125] Feng G, Jiang J, Zhao Y, Wang S, Liu B, Yin K, Niu D, Li X, Chen Y, Duan H, Yang J, He J, Gao Y and Wan Q 2020 *Adv. Mater.* **32** 1906171
[126] Mao J Y, Hu L, Zhang S R, Ren Y, Yang J Q, Zhou L, Zeng Y J, Zhou Y and Han S T 2019 *J. Mater. Chem. C* **7** 48
[127] Hu W, Jiang J, Xie D, Liu B, Yang J and He J 2019 *J. Mater. Chem. C* **7** 682
[128] Zhu L Q, Wan C J, Guo L Q, Shi Y and Wan Q 2014 *Nat. Commun.* **5** 3158
[129] Wan Q, Sharbati M T, Erickson J R, Du Y and Xiong F 2019 *Adv. Mater. Technol.* **4** 1900037
[130] Zhou Z, Yin B and Michel J 2015 *Light Sci. Appl.* **4** e358